nature communications

Article

https://doi.org/10.1038/s41467-025-61753-7

Pathways and selectivity of Fenton degradation of different precursor species of dissolved organic matter

Received: 27 August 2024

Accepted: 27 June 2025

Published online: 10 July 2025

Check for updates

Qi Chen[1], Fan Lü[1,2], Junjie Qiu[1], Hua Zhang[1,2] & Pinjing He[1,2]

Fenton has become one of the dominant technologies for the treatment of recalcitrantly degradable wastewater. Fenton reaction inevitably generates massive amounts of secondary dissolved organic matter (DOM). However, the pathways and selectivity of reaction remain unclear when Fenton is applied in a complex environmental system with different DOM molecules. Here, we design five levels of Fenton reactions based on typical precursor monomers of different DOM species and their stable isotope-labeled monomers combined with actual DOM media. The molecular information of the Fenton-derived DOM for all reactions is obtained based on ultra-high resolution mass spectrometry. The exact mass difference calculations demonstrate that Fenton degrades eight DOM precursor species by different pathways. The temporal gradient changes in the co-molecular characteristics of the Fenton-derived DOM between individual monomer reactions and gradient mixed monomer reactions confirm Fenton degradation selectivity toward eight DOM precursor species. These findings may provide a theoretical basis for using the Fenton process in the targeted degradation of organics.

Fenton is one of the few engineered advanced oxidation processes for the treatment of recalcitrantly degradable wastewater, e.g., landfill leachate[1]. Recalcitrantly degradable wastewater is usually dominated by diverse DOM species[2,3]. DOM is mainly generated by microbial metabolic processes[4] and can be classified into different species, e.g., lipids, proteins, lignins/carboxylic rich alicyclic molecule (CRAM) organics, etc. [5]. In fact, DOM molecules in different DOM-rich media, even in natural organic matter, are almost always the products of diverse biotic and abiotic reactions of homologous monomers. The structural properties of DOM molecules are very complex and media specific, including the rich diversity of carbon skeleton structures (quaternary carbons)[6] and functional groups, which often brings great challenges to the study of specific compounds in actual DOM media[7–9]. The active substances in the Fenton system are very complex, containing not only •OH with a strong oxidation potential, but also generating $O_2^{\bullet-}$ and even high valent Fe species (Fe(IV)), but the oxidation potential of the latter are less than that of •OH[10]. Previous studies have confirmed that the chain reactions initiated by Fenton in recalcitrantly degradable wastewater produce a large number of secondary Fenton-derived DOM molecules, which exhibit substantial differences at the molecular level[11–14]. Therefore, the Fenton degradation efficiency of different DOM molecules determines the abundance of secondary Fenton-derived DOM species, which may pose ecological safety risks. Although, existing studies still stopped at illustrating DOM degradation by Fenton as a whole, and did not dissect the degradation characteristics of each DOM species, understanding the degradation preference of Fenton is essential to precisely control DOM degradation and support the development of affordable, eco-friendly, and highly efficient technology. Thus, the degradation pathways and selectivity of Fenton reaction on different DOM species must be determined. Meanwhile, in terms of environmental and human risks, the toxicological properties of Fenton-derived DOM molecules generated by Fenton system should be determined, but they have rarely been reported to date.

[1]Institute of Waste Treatment & Reclamation, College of Environmental Science and Engineering, Tongji University, Shanghai, China. [2]Shanghai Institute of Pollution Control and Ecological Security, Shanghai, China. e-mail: solidwaste@tongji.edu.cn

Conversely, Fenton-derived DOM molecules are characteristic products of the Fenton reaction and may be the breakthrough in detecting its reaction pathway and selectivity in complex mixed systems. Together with the support of stable isotope tracer techniques, can further validate the results in actual complex media[15,16]. In general, the approach refers to characterizing the Fenton-derived DOM generated via Fenton reactions by ultra-high resolution mass spectrometry (UHRMS) in different environmental media, such as wastewater[14], oceans[17,18], etc. However, current studies have explained the role of Fenton reaction mainly through the relative abundance of DOM species visualized in a van Krevelen diagram (VKD), i.e., the space formed by H/C and O/C[19,20], which has gradually evolved from the traditional five to eight species[19,21–23]. Since DOM substrates for the Fenton reaction are mixed in the natural environment, such methodology cannot supply direct evidence but simply provide tentative indications of organic matter type, functional group, and molecular weight based on correlation analysis[12,14,19]. Furthermore, VKDs have a large amount of overlapping molecular information as well as boundary molecular information[5], which inevitably leads to inaccurate presumptions about Fenton selectivity. Moreover, the molecular information obtained by UHRMS ($C_cH_hO_oN_nS_s$) clearly expresses the reaction products of •OH and helps to infer its reaction pathway, which can also well distinguish the interference of other active species.

To address the above challenge, an approach combining the characteristics of top-down and bottom-up methodologies was developed. Fifty-five typical homologous precursor monomers of different DOM species in complex DOM media were selected and subjected to three types of reaction, namely, individual monomer reaction, mixed monomer reaction, and gradient mixed monomer reaction, including species and time gradients. The Fenton reaction was provided by the classical homogeneous Fe(II)/H_2O_2 system. The present study characterizes the Fenton-derived DOM molecules of different DOM species based on individual monomer and mixed monomer reactions using molecular information obtained by ultra-high-performance liquid chromatography coupled with hybrid quadrupole Orbitrap mass spectrometry (UHPLC Orbitrap MS/MS). The exact mass differences between the Fenton-derived DOM molecules from the individual monomer reactions and monomers were compared to explore the transformation pathways of different DOM species and the toxicological properties of the Fenton-derived DOM molecules. Meanwhile, unidirectional tracer and bidirectional tracer reactions of stable isotope-labeled monomers and Fenton actives were used to validate the transformation pathways of different DOM species in actual complex media, i.e., Suwannee River natural organic matter (SRNOM). The degradation selectivity of Fenton toward different DOM species was explored using the co-molecular characteristics of the DOM molecules derived from individual monomer reactions versus those derived from gradient mixed monomer reactions, including stable isotope monomers. The study findings provide a theoretical basis for Fenton process, which may enhance the targeting of contaminants for removal and lead to fundamental optimization of treatment processes and precise control.

Results and discussion

Fenton-derived DOM of different DOM species

Different DOM species in the individual monomer reaction had different dissolved organic carbon (DOC) concentrations after the Fenton reaction, in which lipids, unsaturated hydrocarbons and aromatic organics exhibited significantly lower abundance than other species ($p < 0.0001$, $p < 0.001$, and $p < 0.001$, respectively) (Fig. 1a), mainly due to their low water solubility (Supplementary Table 1). Supplementary Fig. 1 showed the kinetic degradation profiles of DOC in all individual monomer reactions. Among the highly water-soluble DOM species, proteins, amino sugars, and lignins/CRAM organics exhibited a faster kinetic decay than tannins and carbohydrates, which may indicate differences in the degradation selectivity of the Fenton reaction. However, for DOM species with low water solubility, the kinetic competition did not exhibit any clear pattern. However, DOM molecules derived from carbohydrates were present in significantly lower amounts than other species ($p < 0.05$) (Fig. 1b), suggesting possibly that Fenton does not preferentially attack carbohydrates despite their high hydrophilicity (log D(5.5) = −2.83 to −1.25) (Supplementary Table 1). Notably, the number of vacancies in the benzene ring with homologous groups and the occupation of electron-donating groups (−OH) on the benzene ring directly determined the number of Fenton-derived DOM molecules (Supplementary Fig. 2). For example, the numbers of DOM molecules derived from catechol and phloroglucinol (10 and 26, respectively) were much higher than that from pyrogallol (5), which was mainly due to vacancies providing pathways for the electrophilic addition of •OH and the three adjacent −OH groups of pyrogallol (C (1, 2, 3)) forming three intramolecular hydrogen bonds, thus creating directional barriers to the carbon-shielding effect that stabilized the molecule[24,25].

The DOC concentrations in the mixed monomer reaction showed a similar trend to those of the individual monomer reaction described above. The kinetic degradation profiles of the mixed monomer reaction in Supplementary Fig. 1 also further confirmed the corresponding conclusion for the individual monomer reaction. Similarly, the differences in Fenton-derived DOM for the mixed monomer reaction were comparable to the individual monomer reaction, with significantly more DOM molecules from lipids, proteins, lignins/CRAM organics, and aromatic organics than from the other species ($p < 0.05$). Unexpectedly, the number of molecules derived from unsaturated hydrocarbons and amino sugars was higher than that from tannins and carbohydrates ($p < 0.05$), which clearly differed from the individual monomer reaction.

Subsequently, the molecular properties of the Fenton-derived DOM were explored. The aromatic index (AI) and modified aromatic index (AI_{mod}) can reflect the proportion of heteroatoms in the derived DOM molecules, which helps to indirectly infer the transformation pathways. The results of the individual monomer reaction indicated that the AI of Fenton-derived DOM from tannin and aromatic organics was significantly higher than that of other species ($p < 0.05$), and the AI_{mod} showed the same trend. This finding implied that the DOM derived from tannins have a low proportion of heteroatoms and strong electronic delocalization (Fig. 2a)[26]. The mixed monomer reactions showed similar results (Fig. 2b). The comparative analysis of the AI and AI_{mod} of the monomers of different DOM species and their Fenton-derived DOM molecules revealed that the AI or AI_{mod} of DOM molecules derived from all DOM species except unsaturated hydrocarbons and aromatic organics were significantly higher than that of the monomers themselves ($p < 0.05$), which implied that the monomers of the majority of the DOM species have had their heteroatomic groups removed or non-heteroatomic groups added in the Fenton reaction (Fig. 2a, Supplementary Fig. 3 and Supplementary Table 2).

Redundancy analysis based on the mass-to-charge ratio (m/z) and retention time (RT) of the Fenton-derived DOM of different species from the mixed monomer reactions showed clear commonalities, e.g., lignins/CRAM organics and amino sugars, aromatic organics and unsaturated hydrocarbons, proteins and tannins (Fig. 2c). In addition, the saturation and aromaticity of the Fenton-derived DOM molecules were further categorized based on the VKD (Supplementary Method 1). The Fenton-derived DOM did not contain saturated-like species but rather highly unsaturated- and aromatic-like species, and even the DOM derived from tannins, carbohydrates, and aromatic organics was dominated by polycyclic aromatic-like species, which aptly explained the distributional characteristics of AI and AI_{mod} (Fig. 2d).

The above results suggested that differences in the degradation pathways and degradation selectivity of Fenton for different DOM species at the same reaction concentration were responsible for the observed differences in the Fenton-derived DOM. In addition, unlike

https://doi.org/10.1038/s41467-025-61753-7

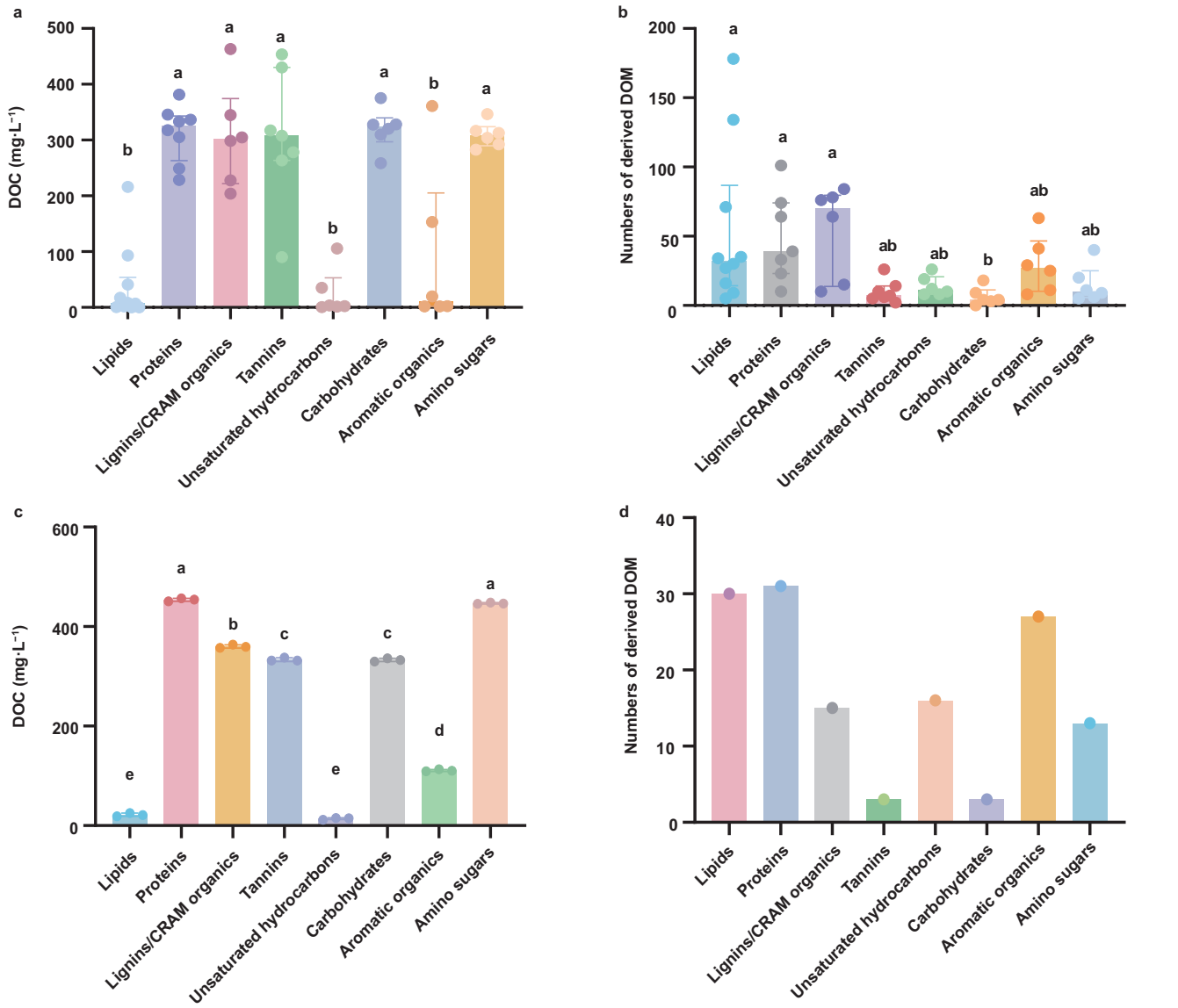

Fig. 1 | DOC and numbers of Fenton-derived DOM molecules after individual monomer reactions and mixed monomer reactions of different DOM species. Monomers of different DOM species were used for the reactions (Supplementary Table 1). The reaction duration was 60 min for both the individual monomer reaction and the mixed monomer reaction. **a** The statistical results of the mean effluent DOC from triplicate tests for individual monomer reactions for each DOM species, where the DOC kinetic degradation changes of all reactions were shown in Supplementary Fig. 1. The bar + data overlap plot shows the median (bar), whiskers representing 1.5 × the interquartile range, and outliers as points beyond the whiskers. **b** The statistical results of the number of Fenton-derived DOM for individual monomer reactions for each DOM species, where the results for each monomer were shown in Supplementary Fig. 2. The bar + data overlap plot shows the median (bar), whiskers representing 1.5 × the interquartile range, and outliers as points beyond the whiskers. The vertical axis represents absolute number. **c** The effluent DOC of mixed monomer reactions for each DOM species, where the results of triplicate tests for DOC were shown. The bar + data overlap plot shows the mean (bar), error bars representing standard deviation from triplicate tests. In addition, the DOC kinetic degradation changes of all reactions were shown in Supplementary Fig. 1. **d** The number of Fenton-derived DOM for mixed monomer reactions of each DOM species. The symbols and bars represent the same values. The vertical axis represents absolute number. The significant differences for statistical hypothesis tests in all panels were labeled using the letter labeling method. The methods and *p*-values for statistical hypothesis tests in all panels were shown in the Source Data file.

the hypothesis of previous studies on Fenton reactions in recalcitrantly degradable wastewater[13,27,28], lignins/CRAM organics were not a key source of the Fenton-derived DOM from the individual or mixed monomer reaction. This was mainly due to the large number of low molecular–weight organic acids, etc., in the complex system, which greatly contributed to the degradation of lignins/CRAM organics by Fenton.

Transformation pathways for DOM species

Fenton system not only catalyzes the production of •OH, but also further produces superoxide radicals and tetravalent iron reactive species. With the development of chemical probe technology, free radical yields in advanced oxidation systems can be accurately measured[29,30]. However, it has been clearly confirmed that •OH are absolutely dominant in the Fenton system under the reaction conditions of the present study, i.e., pH = 3, and that other radicals can be neglected[31,32]. Moreover, UHRMS can easily capture the molecular information of •OH oxidation products[28,33–38]. Therefore, the transformation pathway of DOM in Fenton system was analyzed based on •OH. Currently, UHRMS combined with exact mass difference calculations can accurately capture derived DOM molecules that undergo only zero-order reactions, but derived DOM molecules involved in

https://doi.org/10.1038/s41467-025-61753-7

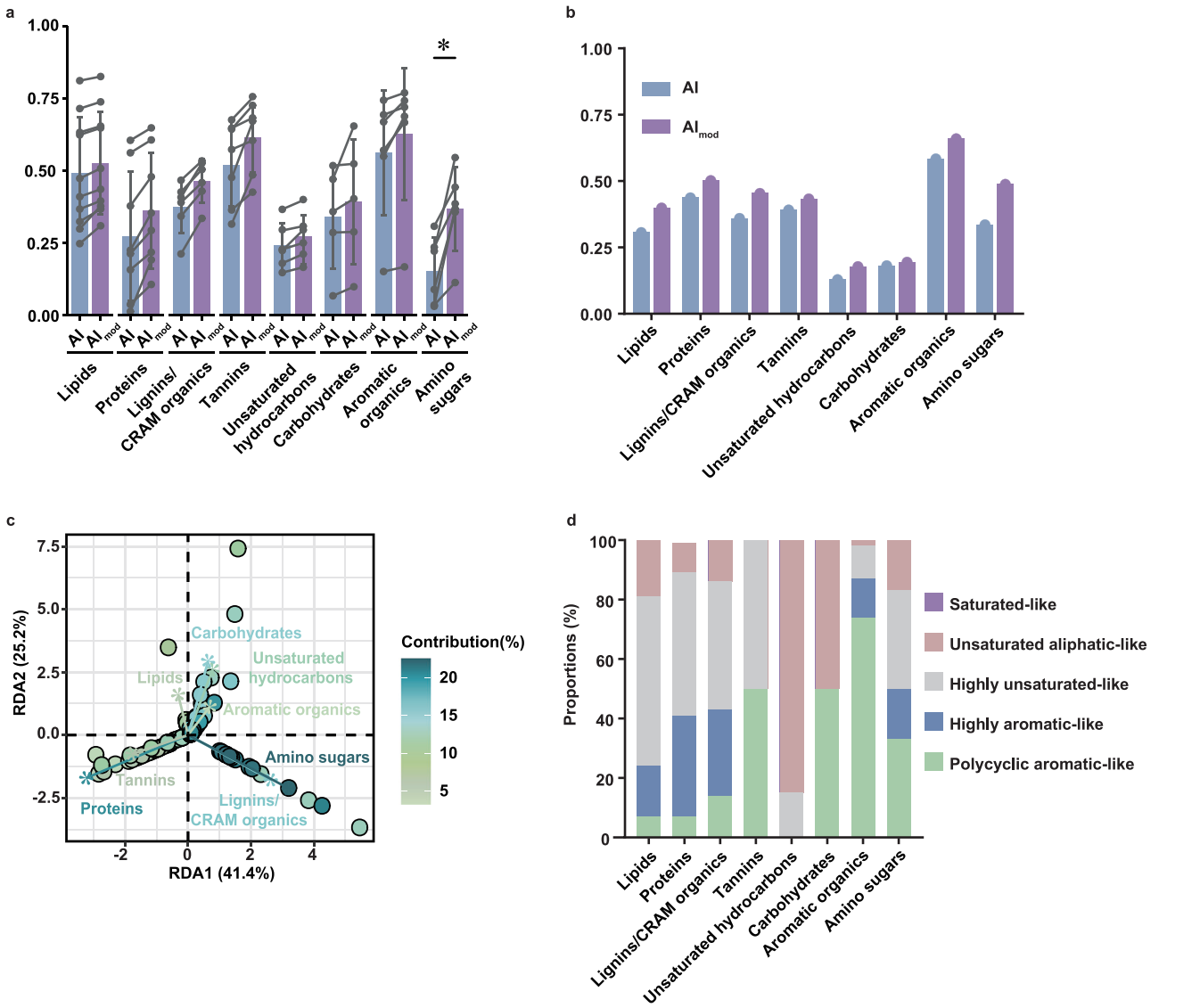

Fig. 2 | Molecular properties of Fenton-derived DOM for Fenton reactions of different DOM species. a AI and AI_{mod} statistics for individual monomer reaction (peak-weighted averages), where AI_{mod} is the modification of AI based on the weights of the oxygen atoms, by toning down the weights of the oxygen atoms (from 1 to 0.5) to more closely match the actual contribution of the heterocyclic conjugated structure. The bar + data overlap plot shows the median (bar), whiskers representing 1.5 × the interquartile range, outliers as points beyond the whiskers and the connecting lines between the AI and AI_{mod} data points representing the same individual monomer reaction. **b** AI and AI_{mod} for mixed monomer reaction (peak-weighted averages). **c** Redundancy analysis based on Fenton-derived DOM molecular information. **d** Relative abundance of saturation and aromaticity classification of Fenton-derived DOM.

subsequent reactions cannot be captured. Twenty-eight zero-order reaction pathways of 55 monomers in the Fenton reaction system were employed to screen the transformation pathways for the Fenton-derived DOM[36,39], including six major categories, namely, dealkylation, oxygen addition, reactions of carboxylic acid, amine, and sulfate, and other reactions (Fig. 3). The transformation pathways of the Fenton-derived DOM were screened based on exact mass difference, see Supplementary Method 1 for details.

Specifically, dehydrogenation ($-H_2$) of lipids was dominant, with the H extraction reaction rate from C–H bonds $>10^8\,M^{-1}{\cdot}s^{-1}$[40], while oxygen addition via direct electrophilic additive (+OH), hydration ($+H_2O$), dihydroxylation (+2O), and methyl to carboxylic acid reaction ($-H_2+O_2$) were the other main reaction pathways, with $-H_2+O_2$ being the cause of dehydrocarbon reactions. Amine reactions were advantageous for proteins degradation, especially the oxidative displacement of amine ($-NH_2+OH$) and ammonia elimination ($-NH_3+O$), due to H on –N functional groups being more likely to donate electrons to •OH for extraction[41]. In addition, protein monomers that contained N and S underwent several types of amine reactions but not sulfate reactions, implying that •OH attacked –N functional groups in preference to –S functional groups[26,42]. Tannins, due to their benzene ring as well as their abundance of hydroxyl groups (–OH), gave active sites to •OH, which tended to remove alkyl ($-C_2H_2$) or carboxylic acids (–CO) as a whole. Unsaturated hydrocarbons had more C = C bond sites for •OH addition and were less interfered with by electron-withdrawing groups, making it easier to convert methyl to alcohol ($-CH_2+O$) when •OH addition occurred[42,43]. Since lignins/CRAM organics contain large numbers of unsaturated C = C bonds as well as electron-donating alkyl groups on their benzene or alicyclic rings, they were highly susceptible to oxygen addition (dihydroxylation ($+H_2O_2$) and direct electrophilic additive (+OH)) by •OH, with reaction rates $>10^9\,mol^{-1}{\cdot}dm^3{\cdot}s^{-1}$ [40,44–46], and methyl were ultimately derivatized to

https://doi.org/10.1038/s41467-025-61753-7

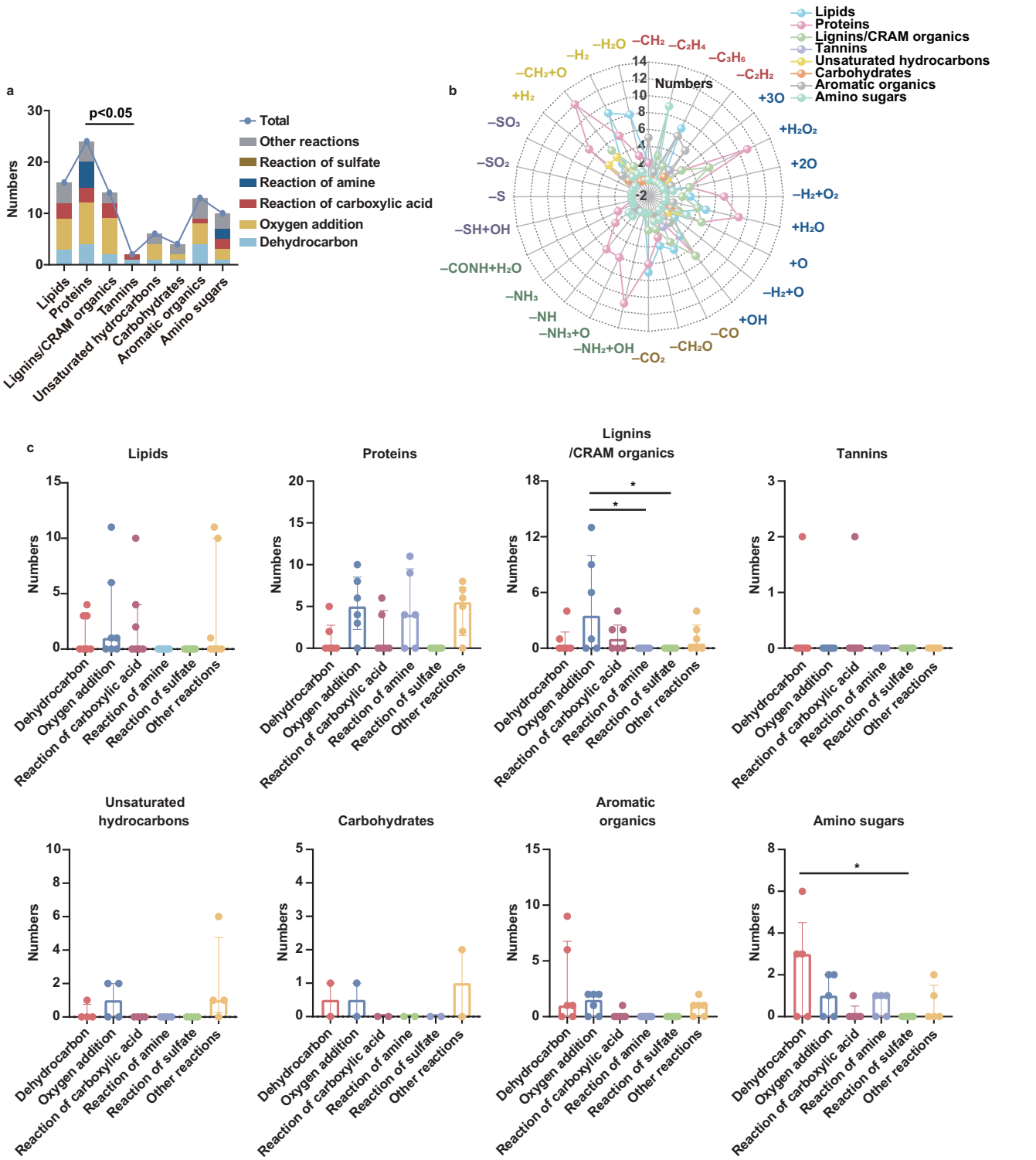

Fig. 3 | Fenton-derived DOM transformation pathways for Fenton (•OH) degradation of different DOM species. Transformation pathways were calculated based on the exact mass difference between Fenton-derived DOM molecules and corresponding monomers for individual monomer reactions of different DOM species. **a** The number of subtype types in the transformation pathway broad categories. **b** The distribution of transformation pathway subtypes. **c** The statistical distribution of transformation pathway subtypes for different DOM species. The bar + data overlap plot shows the median (bar), whiskers representing 1.5 × the interquartile range, outliers as points beyond the whiskers. The axis in all panels represents absolute number. The methods and *p*-values for statistical hypothesis tests in all panels were shown in the Source Data file.

alcohol ($-CH_2+O$). A smaller number of pathways were identified for carbohydrates, probably due to the fact that their abundance of strongly electron-donating hydroxyl groups formed a stable structure by hydrogen bonding to each other and there were virtually no electron-dense benzene rings or double bonds, etc., and, therefore, were less susceptible to attack by •OH. A small number of pathways included dehydrocarbon, oxygen addition, and hydrogenation. •OH degradation of aromatic organic monomers was dominated by the

dehydrocarbon reactions ($p < 0.05$), mainly due to the effects of strong π-bonds on the benzene ring and electron delocalization domains[47], resulting in α-H on the methyl group being the first to be abstracted by •OH and thus the alkyl group being detached[48–50]. Similarly, amino sugars were more inclined to be attacked by •OH via dehydrocarbon reactions ($p < 0.05$), probably due to the strong electron-donating groups −NH and $-NH_2$ on the benzene ring exacerbating the •OH abstraction of the H on the alkyl group[48,51].

In addition, canonical correlation analysis was performed on the transformation pathways of the Fenton reactions of different DOM species with their own physicochemical properties (Fig. 4). Oxygen addition, dehydrocarbon, reaction of carboxylic acid and reaction of amine were closely related to the physicochemical properties of the compounds themselves, with hydroxylation (+O) and low molecular−weight dehydrocarbon reactions ($-CH_2$, $-C_2H_2$) strongly correlated with log K_{oa} and $K_{•OH}$. This finding implied that the above pathways had strong transmedia consistency, i.e., the structural properties of the organic molecules themselves determined their reactivity with •OH[40,42,45]. The reactions responsible for functional group transformations, e.g., methyl to carboxylic acid ($-H_2 + O_2$), alcohol to carboxylic acid ($-H_2 + O$), and carboxylic acid reaction (−CO, $-CH_2O$, $-CO_2$), were strongly correlated with log D(5.5) and log D(7.4), which implied that the abovementioned Fenton reactions and its selectivity were largely determined by the dissociation and partitioning properties of the compounds in the aqueous phase[45,48,49]. In addition, the molecular property indexes H/C made a large contribution to whether •OH underwent direct electrophilic addition. O/C showed a strong correlation with multiple oxygen addition reaction pathways. There was little correlation between amine reactions and the physicochemical properties of the compounds, which may imply that the structural properties of the compounds themselves, e.g., the −N functional groups, determined reaction with •OH[51]. However, the double bond equivalent (DBE) was closely related to the combination of amine reactions with electrophilic addition by •OH ($-NH_3$, $-NH_3 + O$, $-NH_2 + OH$), implying that the presence of amino groups on the unsaturated bond made the molecules susceptible to •OH addition[51].

Validating transformation pathways of DOM species in SRNOM

In order to validate the transformation pathways of Fenton (•OH) degradation of different DOM species in actual complex media, this study further mined comprehensively through stable isotope unidirectional tracer reactions (Fenton + δ^{13}C/δD-monomers + SRNOM) and bidirectional tracer reactions (•OD + δ^{13}C/δD-monomers + SRNOM) in natural organic matter (SRNOM). Both unidirectional tracer reactions and bidirectional tracer reactions added 1–5 δ^{13}C/δD-monomers of eight DOM species to SRNOM as their tracers (Supplementary Table 3), and set up Fenton and •OD reactions of SRNOM without stable isotope-labeled monomers as control subjects (triplicate parallel reactions), respectively. When performing the transformation pathway calculations, the DOM molecular information derived from the above control subjects was deducted, and the remaining DOM molecular information was considered to be that derived from stable isotope-labeled monomers (δ^{13}C/δD-Fenton derived DOM) and used as the typical molecular information derived from the corresponding DOM species. The transformation pathway calculations took into account the case of •OD addition reactions and reactions involving ^{13}C in the δ^{13}C-monomers, where the exact mass of δD was 2.014102 and the exact mass of δ^{13}C was 13.003355.

Figure 5 showed the results of the transformation pathways of different DOM species during the degradation of SRNOM by Fenton (Fig. 5a, b) and •OD (Fig. 5c, d), respectively. The results of the Fenton-derived DOM molecular transformation pathway for different DOM species were highly consistent in both tracer reactions and showed a high degree of similarity to the results of the monomer reactions. Similar to the monomer reactions, both unidirectional and bidirectional tracer reactions showed that dehydrogenation ($-H_2$) and oxygen addition reactions of lipids were the more identified reaction pathways, while dehydrocarbon ($-C_2H_4$, $-C_3H_6$) and reaction of carboxylic acid ($-CH_2O$) were also identified, which were mainly attributed to the overall detachment of the alkyl, carboxyl and carbonyl groups of lipids when they were attacked by the H-abstraction of •OH due to the interference of the neighboring electron-withdrawing groups[40]. The amine reaction of proteins was more dominant in both tracer reactions than in the monomer reactions, especially in the bidirectional tracer reactions ($p < 0.05$). Unlike the monomer reactions, proteins were identified with more sulfate reactions, especially desulfhydryl group (−S) and oxidative displacement of sulfhydryl (−SH + OH), in both tracer reactions of SRNOM. The fact that proteins are rich in −S functional groups and the sulfate reaction in SRNOM were identified by the probe not only demonstrated the effectiveness of stable isotope probes but also the preference of •OH for attacking molecules with strong electron-donating groups, such as −S and −N functional groups[41,51]. In addition to the highest abundance oxygen addition reactions, lignins/CRAM organics was also identified with high abundance of dehydrocarbon, dehydrogenation as well as oxidative methyl to alcohol in both tracer reactions as compared to the monomer reactions. This may be due to the molecular diversity of lignins/CRAM organics in SRNOM and its structural diversity. Because these organics contain not only strong electron-withdrawing groups such as carboxyl groups but also electron-donating groups such as hydroxyl groups, which makes the electron density susceptible to interference of other substance molecules[48,52]. In addition, the results of the transformation pathways of tannins, unsaturated hydrocarbons, aromatic organics, and amino sugars in the two tracer reactions were consistent with the monomer reactions. Unlike the monomer reactions, carbohydrates in the two tracer reactions showed a preference for its transformation pathway, which was dominated by dehydrocarbon ($-CH_2$) and dehydration($-H_2O$). It was mainly due to the fact that the molecular conformation of carbohydrates in complex media changes, exposing more reactive reaction sites (hydroxyl group)[53], which increases their attack by •OH.

Selectivity of Fenton degradation of DOM species

The preference of Fenton reaction to degrade different DOM species in complex systems was difficult to draw definitive conclusions from existing analytical methods, whether VKD or density functional theory. Due to the limitation of solvent effects, the traditional kinetic competition is not applicable to the study of degradation selectivity of DOM species with different water solubilities in the aqueous phase. However, theoretical chemical studies have been carried out to confirm that the selectivity of •OH in the aqueous phase is mainly determined by the structural properties of the organics themselves, e.g., linear free energy relationships[54–56]. In this study, the molecular information of Fenton-derived DOM, a characteristic product of the Fenton reaction, was used to infer the degradation selectivity and preference of Fenton. The Fenton-derived DOM molecular information for the gradient mixed monomer reactions was compared and screened against the Fenton-derived DOM molecular information for the corresponding individual monomer reactions to obtain the same molecular information (co-molecular characteristics). In this study, stable isotope tracing was further utilized to excavate the co-molecular characteristics of the δ^{13}C/δD-containing Fenton-derived DOM molecular information of the gradient mixed monomer reaction and the corresponding individual monomer reactions to confirm the accuracy of the results.

The DOC concentrations for the seven gradients of Fenton reactions decreased with time and then stabilized (Supplementary Fig. 4). In addition, AI and AI_{mod} of the Fenton-derived DOM gradually increased over time in the seven gradients of the Fenton reaction, especially the gradients with more species (Supplementary Fig. 5). This

https://doi.org/10.1038/s41467-025-61753-7

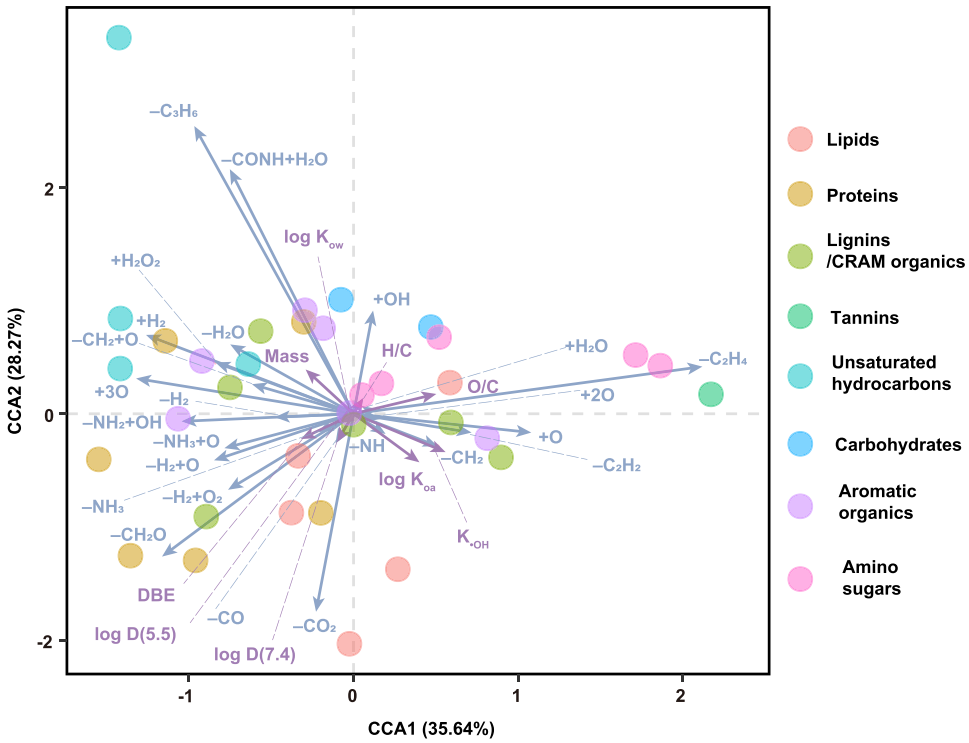

Fig. 4 | Canonical correlation analysis of the physicochemical properties of different DOM species of monomers in Fenton reaction and their transformation pathways. The transformation pathway was the weighted average of its identified abundance in different DOM species and its exact mass. The physicochemical properties of the monomers of different DOM species were shown in Supplementary Table 1.

finding implied a gradual decrease in the proportion of heteroatoms in Fenton-derived DOM molecules[57], which was closely related to the aforementioned attack pathway of •OH.

Further, the identification of Fenton-derived DOM molecular characteristics common to individual monomer reactions in gradient mixed monomer reactions enabled the reaction selectivity to be determined from the change in their number over the temporal gradient. In addition, the accuracy of determining Fenton selectivity using changes in the time gradient of the co-molecular characteristics described above was further confirmed by stable isotope tracer techniques. The results indicated that Fenton degradation of proteins was preferred over that of carbohydrates (Fig. 6a) owing to the fact that both were rich in hydroxyl and amino groups, respectively, but the amino group had a stronger electron-donating ability than the hydroxyl group, while the •OH prefers to be the first to attack the strong electron-donating group[45]. The results for $\delta^{13}C/\delta D$-containing Fenton-derived DOM molecules verified the accuracy of the above results (Fig. 6b). When unsaturated hydrocarbons were present in the reaction system, its reaction priority and that of proteins was higher than that of carbohydrates (Fig. 6a). The results of $\delta^{13}C/\delta D$-containing Fenton-derived DOM molecules further confirmed that the reaction priority of unsaturated hydrocarbons was higher than that of proteins (Fig. 6b). This is mainly due to the near-diffusive oxygen addition (trihydroxylation (+3O)) rate of •OH to the C = C bonds of unsaturated hydrocarbons ($>10^9\,mol^{-1}{\cdot}dm^3{\cdot}s^{-1}$) with less interference from electron-withdrawing groups[40,44]. Then, when lipids were introduced into the reaction system, both Fenton-derived DOM and $\delta^{13}C/\delta D$-containing Fenton-derived DOM confirmed that the reaction priority of unsaturated hydrocarbons, lipids and proteins was higher than that of carbohydrates (Fig. 6a, b). When tannins were present in the Fenton reaction system, the •OH degradation preference for unsaturated hydrocarbons, lipids and proteins remained higher priority than that for carbohydrates and tannins (Fig. 6a, b). When amino sugars intervened in the Fenton reaction system, both Fenton-derived DOM molecular characteristics and $\delta^{13}C/\delta D$-containing Fenton-derived DOM molecular characteristics revealed that the reaction priority of unsaturated hydrocarbons, proteins, lipids, and amino sugars was higher than carbohydrates and tannins, meanwhile, the Fenton-derived DOM molecular characteristics revealed that the •OH degradation preference for tannins exhibited a higher priority than carbohydrates (Fig. 6a, b). This is mainly due to the fact that tannins contain π-electron cloud-rich benzene rings with high electron density compared to carbohydrates, whereas •OH is strongly electrophilic and it attacks tannins preferentially[49,50,58]. Figure 6a further showed that when lignins/CRAM organics intervened in the reaction system, unsaturated hydrocarbons, proteins, lipids, amino sugars and lignins/CRAM organics have a higher reaction priority than tannins and carbohydrates, and the results of the $\delta^{13}C/\delta D$-containing Fenton-derived DOM molecular information further revealed that lignins/CRAM organics had a lower reaction priority than unsaturated hydrocarbons, proteins, lipids, and amino sugars but a higher priority than tannins and carbohydrates. This is mainly due to the carboxyl group (−COOH), a strong electron-withdrawing substituents in lignins/CRAM organics, which is not easily attacked by •OH as compared to amino, hydroxyl and other electron-donating substituents in proteins and amino sugars[48]. However, the presence of −COOH will make the neighboring C−H bond become more active, and the multi-hydroxyl structure of tannin, especially the ortho and neighboring hydroxyl groups will form a conjugation effect[59], which makes the tannins less susceptible to attack. When species pertaining to the eight species were present, •OH further demonstrated its potential to selectively attack different DOM species. Unsaturated hydrocarbons, proteins, lipids, amino sugars and lignins/CRAM organics showed a higher reaction preference than aromatic organics, tannins and carbohydrates, whereas the degradation preference of •OH for aromatic organics was prioritized over tannins and carbohydrates (Fig. 6a). The $\delta^{13}C/\delta D$-containing Fenton-

https://doi.org/10.1038/s41467-025-61753-7

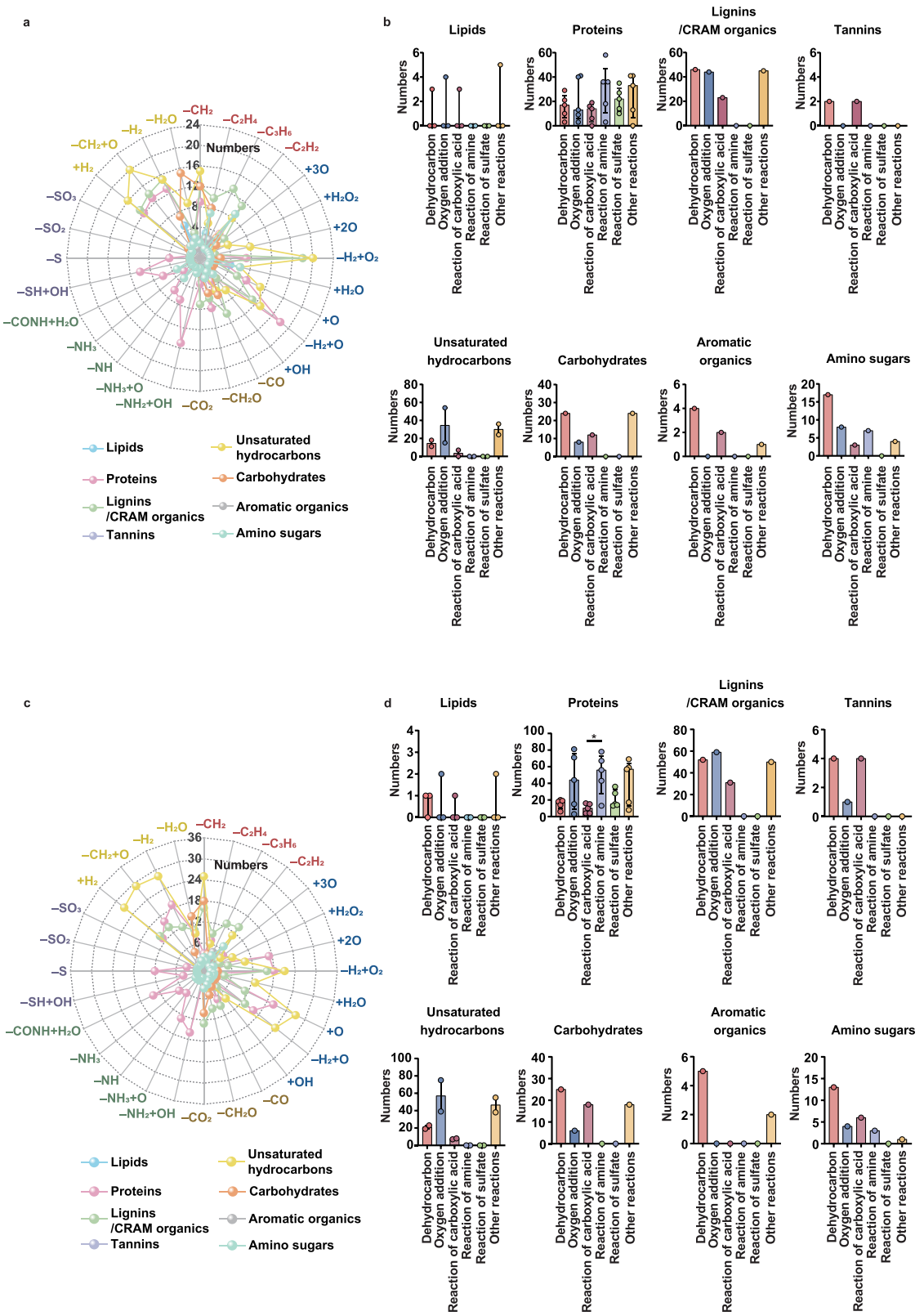

derived DOM molecule confirmed these results (Fig. 6b). Aromatic organics contain abundant fused benzene rings and benzo-fused ring systems, even though they have high electron densities, they are prone to make the π-electron cloud to produce conjugation effects, or even to form a rigid structure[59,60], which is not easily attacked preferentially by •OH, e.g., fluorenone is a typical benzo-fused ring systems and contains carbonyl group (C = O) with a high electron density, and even though C = O provides a high active site, the conjugation effect disperses the electron density of its[61]. Thus, this explains the degradation priority of aromatic organics among different DOM species. In summary, the selectivity of Fenton degradation on different DOM species was roughly in the following order: unsaturated hydrocarbons > lipids = proteins > amino sugars > lignins/CRAM organics > aromatic organics > tannins > carbohydrates.

https://doi.org/10.1038/s41467-025-61753-7

Fig. 5 | Transformation pathways of different DOM species in unidirectional tracer reactions and bidirectional tracer reactions of SRNOM. Unidirectional tracer reactions: Fenton + $\delta^{13}C/\delta D$-monomers + SRNOM; Bidirectional tracer reactions: •OD + $\delta^{13}C/\delta D$-monomers + SRNOM. Transformation pathways were calculated based on the exact mass difference between Fenton-derived DOM molecules and corresponding $\delta^{13}C/\delta D$-monomers for different DOM species. The transformation pathway calculations took into account the case of •OD addition reactions and reactions involving ^{13}C in the $\delta^{13}C$-monomers, where the exact mass of δD was 2.014102 and the exact mass of $\delta^{13}C$ was 13.003355. **a** The distribution of transformation pathway subtypes in the unidirectional tracer reactions. **b** The statistical distribution of transformation pathway subtypes for different DOM species in the unidirectional tracer reactions. The bar + data overlap plot shows the median (bar), whiskers representing 1.5 × the interquartile range, outliers as points beyond the whiskers. **c** The distribution of transformation pathway subtypes in the bidirectional tracer reactions. **d** The statistical distribution of transformation pathway subtypes for different DOM species in the bidirectional tracer reactions. The bar + data overlap plot shows the median (bar), whiskers representing 1.5 × the interquartile range, outliers as points beyond the whiskers. The axis in all panels represents absolute number. The methods and *p*-values for statistical hypothesis tests in all panels were shown in the Source Data file.

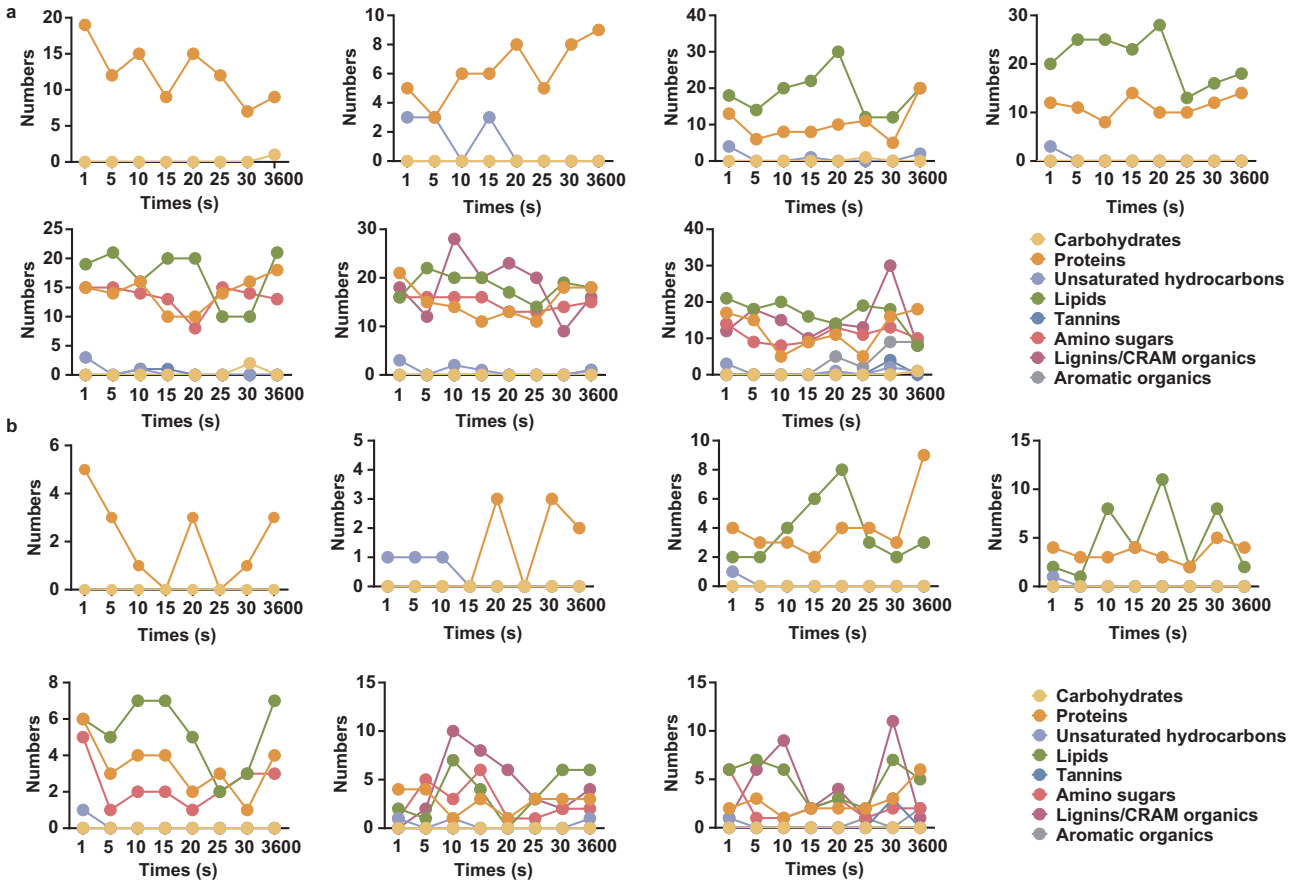

Fig. 6 | Number of co-molecular characteristics of derived DOM from Fenton degradation of different DOM species in the gradient mixed monomer reactions versus individual monomer reactions. a The co-molecular characteristics of Fenton-derived DOM in the gradient mixed monomer reactions versus individual monomer reactions. **b** The co-molecular characteristics of stable isotope-containing Fenton-derived DOM ($\delta^{13}C$ and δD) in the gradient mixed monomer reactions versus individual monomer reactions. In order to visualize the differences, nonequally-spaced time points in the horizontal coordinate were presented in equal proportions. The vertical axis in all panels represents absolute number.

Toxicological properties of Fenton-derived DOM molecules

Fenton have been shown to derive large numbers of DOM molecules. The toxicological properties of the Fenton-derived DOM molecules of different species origins warrant more attention to support the targeted removal of DOM species. The toxicological properties of the Fenton-derived DOM molecules in the identified transformation pathways (Supplementary Table 4) were further explored and classified via in vitro and in vivo assays. The in vitro data of Tox21 10 K, which are based on quantitative high-throughput screening (qHTS) of predicted chemical responses in humans based on their activity profiles and gene symbol hits, were employed in this classification[62–64]. The starting concentration range for in vitro qHTS of the Fenton-derived DOM molecules was 0.016–69,830.4 μg·L^{-1} (half-maximal activity concentration, AC_{50}, Supplementary Table 5). In comparison, the reported concentrations of DOM molecules in organic wastewater (pharmaceutical wastewater, landfill leachate, industrial wastewater, etc.) after Fenton process, used either as a pretreatment, deep treatment, or full flow, were within or even much higher than this range (above mg·L^{-1} level)[65,66]. The relative abundance of DOM molecules derived from lipids and aromatic organics with identified in vitro toxicity endpoints was significantly higher ($p < 0.05$) than that from other species, with hit rates as high as 29.76% and 93.19% in the activity assay, respectively (Fig. 7a, b and Supplementary Table 5). In addition, the variety of Tox21 10 K gene symbol hits for DOM molecules derived from lipids and aromatic organics was higher than that of the other species, implying a broader pathway for their attack on human genes. Notably, the DOM molecules derived from amino sugars were not screened in the in vitro qHTS assays. The highest numbers of gene

https://doi.org/10.1038/s41467-025-61753-7

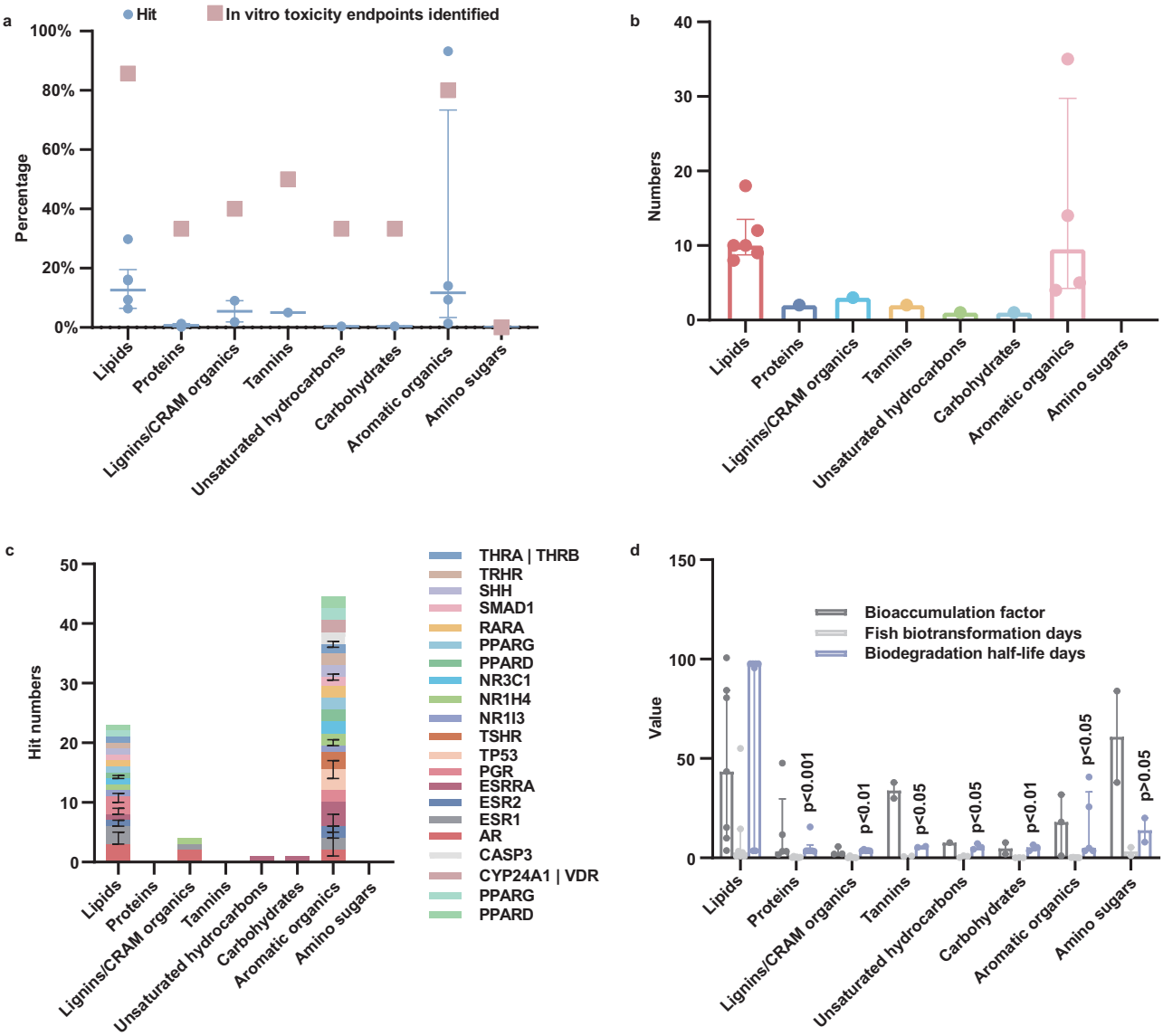

Fig. 7 | Results of environmental and human risk assessment of Fenton-derived DOM molecules from different DOM species degraded by Fenton. a Relative abundance of derived DOM molecules that identified in vitro toxicity endpoints (red square scatters) and their proportion of all in vitro toxicity assays that hit toxicity endpoints (blue circular scatters). The median (center lines), 1.5 × the interquartile range (whiskers), and outliers (points beyond the whiskers) for the blue circular scatters are shown synchronously in the panel. **b** Numbers of types of gene symbol hits in Tox21 10 K activity assays. The bar + data overlap plot shows the median (bar), whiskers representing 1.5 × the interquartile range, outliers as points beyond the whiskers. The vertical axis represents absolute number. **c** Different kinds of gene symbol hits in Tox21 10 K activity assays, where only gene symbols with more than two hits for derived DOM molecules in each DOM species were shown. All gene hit symbols and number of hits were shown in Supplementary Table 6. The small bars in the stacked bars represent the median and the whiskers at the top of each small bar represent 1.5 × the interquartile range. The vertical axis represents absolute number. **d** In vivo assay data including bioaccumulation factor, fish biotransformation days, and biodegradation half-life days. The bar + data overlap plot shows the median (bar), whiskers representing 1.5 × the interquartile range, outliers as points beyond the whiskers. The methods and *p*-values for statistical hypothesis tests of biodegradation half-life days for different DOM species were shown in the Source Data file.

symbol hits (Tox21 10 K) for different species of Fenton-derived DOM molecules were androgen receptor, estrogen receptor 1, estrogen receptor 2, estrogen related receptor α, and progesterone receptor (Fig. 7c and Supplementary Table 6). In addition, the results of the above in vitro assays were combined with in vivo assay results and environmental properties. The bioaccumulation factors of DOM molecules derived from lipids, tannins, and aromatic organics were higher than those of other species, and the biodegradation half-life days of DOM molecules derived from lipids was significantly higher than that from other species ($p < 0.05$), which implied that these molecules had higher environmental accumulation properties and higher risk of human intake (Fig. 7d and Supplementary Table 5). Fish biotransformation days of Fenton-derived DOM molecules from different DOM species did not show statistical differences. Unexpectedly, DOM molecules derived from amino sugars possessed high bioaccumulation factors, but the hit gene symbols were not identified in the in vitro qHTS assays. Overall, DOM molecules derived from lipids and aromatic organics posed high environmental and human risks.

In addition, this study further mined the in vitro and in vivo assay toxicity data of monomers of different DOM species (Supplementary Fig. 6 and Supplementary Tables 7 and 8) and comparatively analyzed the changes in toxicity properties of monomers and derived DOM molecules before and after Fenton reaction. There were no in vitro qHTS assay data identified for all monomers of lignins/CRAM organics

(Supplementary Fig. 6 and Supplementary Tables 7 and 8). The Fenton-derived DOM molecules of all DOM species except lipids, lignins/CRAM organics and aromatic organics had fewer hit gene symbol types than their corresponding monomers (Fig. 7c and Supplementary Fig. 6), which implied that the bioactivity of all DOM species except lipids, lignins/CRAM organics and aromatic organics was decreased after Fenton reaction. As far as the in vivo assay data were concerned, the bioaccumulation factors of the Fenton-derived DOM molecules of the proteins were significantly higher than those of their monomers ($p < 0.01$, Supplementary Fig. 7), while, at the same time, the predicted LC_{50} of fathead minnow was significantly lower than that of their monomers ($p < 0.01$, Supplementary Fig. 7). Fenton-derived DOM molecules of tannins had significantly higher fish biotransformation days than their monomers ($p < 0.05$, Supplementary Fig. 7). The results of the above in vivo assays indicated that the toxicity of the Fenton-derived DOM molecules of proteins and tannins was significantly higher than that of the corresponding monomers. In addition, the predicted LC_{50} of fathead minnow of the Fenton-derived DOM molecules of lipids was significantly higher than that of their monomers ($p < 0.05$, Supplementary Fig. 7), and the fish biotransformation days of the Fenton-derived DOM molecules of aromatic organics were significantly lower than that of their monomers ($p < 0.05$, Supplementary Fig. 7). However, there were no statistically significant differences in the in vitro experimental data before and after the Fenton reaction for the lipids and aromatic organics, and their Fenton-derived DOM molecules had more hit gene type and number than the other DOM species. The above results implied that although the toxicity of lipids and aromatic organics decreased after the Fenton reaction, the toxicity of their Fenton-derived DOM molecules remained at high levels. The biodegradation half-life days of all DOM species were not significantly different before and after the Fenton reaction (Supplementary Fig. 7). Overall, the toxicity of proteins and tannins increased after the Fenton reaction, while the toxicity of lipids and aromatic organics remained significant and should not be overlooked.

Limitations and future developments

This study successfully utilized Fenton-derived DOM molecules as a mixed blessing to comprehensively identify the pathways and selectivity of Fenton degradation on different DOM species. The use of typical precursor monomers of different DOM species in actual media may be the first step towards making the "black-box model" transparent. However, the analysis of the transformation pathways and selectivity of Fenton degradation of different DOM species was only based on •OH, and whether the subsequent generation of unspecified reactive substances, such as $O_2^{\bullet-}$, by the Fenton chain reaction would interfere with the above transformation pathways and selectivity still needs to be further investigated. Currently, UHRMS combined with exact mass difference can only calculate the transformation pathways of Fenton-derived DOM molecules that undergo the zero-order reaction and do not participate in the subsequent chain reaction, which is a small number of Fenton-derived DOM molecules. In contrast, most of the Fenton-derived DOM molecules participated in the subsequent chain reaction and their multistage transformation pathways could not be recognized. Further, the effect of possible environmental factors in the actual DOM media, e.g., pH, salinity, etc., on the conclusions of the Fenton pathway and selectivity in this study should be verified in the future. In addition, the toxicological properties of the Fenton-derived DOM molecules were analyzed statistically only based on a large amount of data from Tox21 10 K, and subsequent in vivo and in vitro experiments are still required for validation.

Methods

Monomers

The different DOM species included eight species, namely lipids, proteins, lignins/CRAM organics, tannins, unsaturated hydrocarbons, carbohydrates, aromatic organics, amino sugars[5,19,23]. In this study, 5–10 monomers were selected for each DOM species, specifically 10 lipids, 8 proteins, 7 tannins, 6 each of lignins/CRAM organics, unsaturated hydrocarbons, carbohydrates, aromatic organics, and amino sugars. All of the above monomers are typical homologous precursors of different DOM species in natural organic matter or anthropogenic DOM-rich media. All the monomers were purchased from Shanghai Macklin Biochemical Co., Ltd. and Shanghai Aladdin Biochemical Technology Co., Ltd. Their basic physical and chemical properties were shown in Supplementary Table 1. In addition, to verify the pathways and selectivity of the Fenton reaction in mixed monomers or complex media, this study selected 1–5 stable isotope-labeled monomers (labeled with either $\delta^{13}C$ or δD) corresponding to the monomers of eight DOM species mentioned above for tracing. The stable isotope-labeled monomers were purchased from Sigma-Aldrich, USA and MedChemExpress, USA with stable isotope purity > 98 %, details of which were provided in Supplementary Table 3.

Experimental procedures

Monomer reactions. The Fenton reaction was carried out using the most classical homogeneous system of $FeSO_4$ and H_2O_2, and the specific operation procedure was shown in Supplementary Method 2. Three groups of experiments with DOM species were investigated, including: (i) Individual monomer reaction: 55 typical precursor monomers pertaining to eight DOM species were individually subjected to the Fenton reaction, with an initial addition amount of 1000 mg/L for each monomer. The ratio of the mass concentration of the H_2O_2 to the monomers and the ratio of the molar concentration of H_2O_2 to Fe^{2+} were 1.5:1 and 5:1, respectively. In order to be able to accurately mine the degradation pathways and selectivity of Fenton through the molecular characterization of Fenton-derived DOM as much as possible, the dosage of this Fenton agent was significantly lower than the optimal values of the previous studies[31]. Both $FeSO_4$ and H_2O_2 were dosed once at the beginning of the reaction. The total duration of all the reactions was 60 min, and eight time gradient of samples were taken for each reaction process for the study of kinetic degradation changes, including 1, 5, 10, 15, 20, 25, 30, and 3600 s. (ii) Mixed monomer reaction: The monomers of each species were mixed to carry out the Fenton reaction separately. The monomers of each DOM species were mixed in equal amounts in mass to ensure that the total amount for initial addition remained at 1000 mg/L. The reaction conditions, such as the proportion of Fenton chemical dosage ($FeSO_4$ and H_2O_2), reaction time, chemicals dosage time, and eight time gradient samples collection times were kept consistent with individual monomer reaction. (iii) Gradient mixed monomer reaction: Five monomers were selected for each DOM species for gradient experiments. One to five corresponding stable isotope-labeled monomers were also added to the five monomers of each DOM for Fenton-selectivity tracking and validation. The monomers and corresponding stable isotope-labeled monomers selected for the eight DOM species were shown in Supplementary Tables 3 and 9, respectively. The specific experimental operations were categorized as (1) carbohydrates + proteins; (2) carbohydrates + proteins + unsaturated hydrocarbons; (3) carbohydrates + proteins + unsaturated hydrocarbons + lipids; (4) carbohydrates + proteins + unsaturated hydrocarbons + lipids + tannins; (5) carbohydrates + proteins + unsaturated hydrocarbons + lipids + tannins + amino sugars; (6) carbohydrates + proteins + unsaturated hydrocarbons + lipids + tannins + amino sugars + lignins/CRAM organics; (7) carbohydrates + proteins + unsaturated hydrocarbons + lipids + tannins + amino sugars + lignins/CRAM organics + aromatic organics. In order to capture as much of Fenton's zero-order response as possible, we performed intensive sampling within the first 30 s immediately after the addition of H_2O_2, with a time gradient included: 1, 5, 10, 15, 20, 25 s, 30, and 3600 s. The starting addition of each monomer in each

gradient reaction was 100 mg·L^{-1}, including 1 mg·L^{-1} of the corresponding 1–5 stable isotope-labeled monomer, respectively. Therefore, the dosage of the Fenton chemicals ($FeSO_4$ and H_2O_2) in each gradient reaction was increased with the increase of the starting total addition. Other reaction conditions, such as the proportion of Fenton chemical dosage ($FeSO_4$ and H_2O_2), reaction time, and chemicals dosage time were kept consistent with individual monomer reaction. All of the above reactions were down in single batch as the purity of the monomers were all above 99%. A sample of 0.1 mL on the time gradient was immediately added to 50 mL of ultrapure water (H_2O, Milli-Q, ≥18 MΩ cm) for substantial dilution to quench the Fenton reaction. These operations were performed in order to immediately quench Fenton reaction in the absence of scavengers, as the addition of scavengers would have greatly affected the analysis of the Fenton-derived DOM molecules.

Unidirectional tracer reactions in SRNOM. To further validate the pathway and selectivity of Fenton degradation of actual complex media, we further designed 9 sets of Fenton experiments using SRNOM (2R101N, International Humic Substances Society) as the media, while adding 1–5 stable isotope monomers of each of the eight DOM species for tracing (Supplementary Table 3). The starting concentration of SRNOM for each set of experiments was 1000 mg·L^{-1} (566 ± 12 mg C·L^{-1}), including 10 mg·L^{-1} of each stable isotope monomer (Supplementary Table 3). The addition proportion of Fenton reagents ($FeSO_4$ and H_2O_2), the dosing time, the reaction duration, and the procedure were consistent with those of the monomer reaction described above. A sample of 0.1 mL was added to 50 mL of ultrapure water (H_2O, Milli-Q, ≥18 MΩ cm) for substantial dilution immediately after the Fenton reaction to quench the Fenton reaction. The specific experimental procedures were described in Supplementary Method 3.

Bidirectional tracer reactions in SRNOM. Although UHRMS is able to capture •OH-derived DOM molecules in the Fenton system, this study further attempted to validate the Fenton degradation pathway and selectivity of actual complex media by bidirectional tracing through the stable isotopes of •OH and the stable isotopes of different DOM species. The stable isotope of •OH, •OD, was produced by deep UV excitation of D_2O[67] (≥ 99.95 atom % D, Sigma-Aldrich, USA). Deep UV was provided by a photochemical reactor (AF3, Shanghai 3S Technology Co., Ltd.) equipped with a UV lamp of λ = 254 nm with a power of 15 W and an optical density of 0.58 mW·(cm^2)$^{-1}$. The above photochemical reaction parameters are close to the typical range demonstrated in excited radical reaction studies (optical density: 0.2–0.51 mW·(cm^2)$^{-1}$)[67,68]. The photochemical reactor was equipped with a 6 mL quartz reaction dish with a surface-to-volume ratio of 0.29 cm^2·(cm^3)$^{-1}$, which is within the range of typical values (0.21–0.88 cm^2·(cm^3)$^{-1}$) in photochemical reaction studies[67,69]. Consistent with the nine sets of unidirectional tracer experiments for SRNOM degradation by Fenton described above, nine sets of bidirectional tracer experiments were also set up, with the starting concentration of SRNOM of 1000 mg/L (566 ± 12 mg C·L^{-1}), including 10 mg·L^{-1} of each stable isotope monomer (Supplementary Table 3). In order to capture the zero-order reaction as much as possible, the duration of UV radiation was only 12 h. Immediately after the reaction, a sample of 0.1 mL was added to 50 mL of ultrapure water (H_2O, Milli-Q, ≥18 MΩ cm) and diluted heavily to quench the free radical reaction. The specific procedures for the 9 sets of bidirectional tracer experiments were described in Supplementary Method 3.

Basic physicochemical properties

DOC was measured in all end-of-reaction and process samples. Each sample was measured in triplicate. The detailed measurement method and procedure were shown in the Supplementary Method 4.

Fenton-derived DOM analysis and data mining

All the solid phase extraction (SPE) pretreatment of the Fenton reaction effluents as well as the UHPLC Orbitrap MS/MS (Thermo Fisher Scientific, Inc., USA) testing procedures[70] were described in detail in Supplementary Methods 5 and 6. The purpose of SPE was to remove inorganic salts thereby preventing the risk of column clogging. Mass spectra in the positive ion mode (ESI(+)) were acquired as long as it was due to the fact that a large number of previous studies by ourselves as well as by others confirmed that ESI(+) was able to recognize far more mass spectral information and molecular information than ESI(−)[14,71–73]. In order to accurately identify the stable isotope information of DOM molecules, the following customized data pipeline was used for mass spectrometry data analysis in this study: (1) RAW data were converted to mzXML data format by ProteoWizard MSConvertGUI software[74]; (2) peak picking was performed by the R code enviPick[36] in the RStudio environment (v2023.12.0), which was parameterized as described in Supplementary Method 1; and (3) assignment of molecular formulas and accurate identification of isotope peaks were performed by the R code MFAssignR[37,75] in the RStudio environment (v2023.12.0). The molecular formula assignment criteria for MFAssignR were: $^{12}C_{2-50}{}^{1}H_{2-100}{}^{16}O_{0-30}{}^{14}N_{0-2}{}^{32}S_{0-1}{}^{1}$. Samples to which stable isotope monomers were added were screened twice using the ^{13}C isotope filtration function to obtain molecular information about molecules containing ^{13}C in their molecular formulas, including the exact mass, retention time, and intensity of ^{13}C. In addition, the identification range of D was set to $0 \le D \le 20$ based on the number of D in the stable isotope monomer[67]. Further, DOM molecules with $-10 < DBE\text{-}O < 10$, $0.33 < H/C < 2.5$, $O/C \le 1.2$ were recognized[1], where DBE was the DBEs, and molecular property indexes were calculated as described in Supplementary Eqs. 1–5. Derived DOM molecules that did not satisfy elemental conservation in all monomer reactions were deducted first. Sample mass peaks were discarded whenever they appeared in any of the triplicate blanks. The molecules of their oxidation products namely Fenton-derived DOM were obtained by comparing and screening the m/z and RT of the molecular information before and after the Fenton reaction. The identification of mass tolerance and RT drifting tolerance was shown in Supplementary Method 1. The transformation pathways of Fenton-derived DOM molecules were calculated based on the exact mass differences between them and the monomers, and identified pathways that did not satisfy elemental conservation were subtracted (Supplementary Method 1). All csv data table merging as well as column extraction, splitting and merging were performed in the RStudio environment (v2023.12.0). Redundancy analysis (RDA) was performed in the RStudio environment (v2023.12.0) with the R packages "FactoMineR" and "factoextra", where molecular information was determined based on RT and m/z. Canonical correspondence analysis (CCA) was performed in the RStudio environment (v2023.12.0) with the R package "vegan", in which molecular information was identified based on RT and m/z. The applicability of CCA and RDA was determined by identifying the gradient length of the molecular information response through the "decorana" function before performing CCA analysis. The fitting of the molecular property indexes AI and AI_{mod} on the temporal gradient was performed in the RStudio environment (v2023.12.0) with the R packages "tidyverse", "ggsci", "ggExtra", "ggpmisc", where AI and AI_{mod} were peak-intensity weighted values. The statistical hypothesis testing was used for data analysis and comparisons to reveal statistical significance of the differences, including *t*-test, Mann–Whitney *U* test, Tukey one-way ANOVA, and Dunn's rank test. The saturation and aromaticity of the Fenton-derived DOM were calculated in Supplementary Method 1.

Fenton-derived DOM toxicology analysis

The structure properties and substance identification of the Fenton-derived DOM molecules were analyzed by Compound Discoverer v3.2 (Thermo, USA) software based on MS/MS results, and then the derived DOM molecules that were able to identify the transformation pathway based on the exact mass difference were further analyzed for their toxicological properties. Toxicology analyses included predicted LC_{50} for fathead minnow ($mg{\cdot}L^{-1}$), bioaccumulation factor, development toxicity value, mutagenicity value, bioconcentration factor, fish biotransformation (days), biodegradation half-life (days), and toxicity endpoints and hit gene symbol based on high-throughput analyses where predicted LC_{50} for fathead minnow ($mg{\cdot}L^{-1}$), bioaccumulation factor, development toxicity value and mutagenicity value were calculated by software U.S. EPA Toxicity Estimation Software Tool v5.1.2, while, bioconcentration factor, fish biotransformation (days) and biodegradation half-life (days) were obtained from U.S. EPA CompTox Chemicals Dashboard v2.5.3. In vitro assay data for toxicity endpoints and hit gene symbol based on high-throughput analysis were obtained from U.S. EPA CompTox Chemicals Dashboard v2.5.3, including ToxCast total assay number, hit gene symbol number, hit percentage rate, and the range of concentrations causing half-maximal response (AC_{50}, μg). More importantly, gene symbol of hits and number of hits in Tox21 10 K were analyzed[63,64]. The statistical hypothesis testing was used for data analysis and comparisons to reveal statistical significance of the differences, including *t*-test, Mann–Whitney *U* test, Tukey one-way ANOVA, and Dunn's rank test.

Data availability

All raw mass spectrometry data generated in this study have been deposited in the Figshare repository with identifier (https://doi.org/10.6084/m9.figshare.28190549.v1)[76]. The data generated in this study that support the findings are provided in the main text and Supplementary Information. The source data underlying Figs. 1–7 and Supplementary Figs. 1–7 is provided as a Source Data file.

Code availability

The enviPick code used for peak picking of mass spectrometry data in this study is available in the GitHub repository at https://github.com/blosloos/enviPick. The MFAssignR code used for isotope-accurate identification of mass spectrometry data in this study is available in the GitHub repository at https://github.com/skschum/MFAssignR. The R code generated in this study for data processing and analysis, as described in the "Methods" section, has been deposited in the Figshare repository with identifier (https://doi.org/10.6084/m9.figshare.28190588.v1)[77].

References

1. Qiu, J. J., Lü, F., Li, T. Q., Zhang, H. & He, P. J. A novel 4-set Venn diagram model based on high-resolution mass spectrometry to monitor wastewater treatment. *Environ. Sci. Technol.* **56**, 14753–14762 (2022).
2. McKenna, J. H. DOC dynamics in a small temperate estuary: simultaneous addition and removal processes and implications on observed nonconservative behavior. *Estuaries* **27**, 604–616 (2004).
3. Shon, H. K., Vigneswaran, S. & Snyder, S. A. Effluent organic matter (EfOM) in wastewater: constituents, effects, and treatment. *Crit. Rev. Environ. Sci. Technol.* **36**, 327–374 (2006).
4. Cotrufo, M. F. et al. Formation of soil organic matter via biochemical and physical pathways of litter mass loss. *Nat. Geosci.* **8**, 776–779 (2015).
5. Qiu, J. J., Lü, F., Zhang, H., Shao, L. M. & He, P. J. Data mining strategies of molecular information for inspecting wastewater treatment by using UHRMS. *Trends Environ. Anal. Chem.* **31**, e00134 (2021).
6. Li, S. Y. et al. Dearomatization drives complexity generation in freshwater organic matter. *Nature* **628**, 776–781 (2024).
7. Zark, M. & Dittmar, T. Universal molecular structures in natural dissolved organic matter. *Nat. Commun.* **9**, 3178 (2018).
8. Arakawa, N. et al. Carotenoids are the likely precursor of a significant fraction of marine dissolved organic matter. *Sci. Adv.* **3**, e1602976 (2017).
9. Lehmann, J. & Kleber, M. The contentious nature of soil organic matter. *Nature* **528**, 60–68 (2015).
10. Wang, H. J., Gao, L. W., Xie, Y. X., Yu, G. & Wang, Y. J. Clarification of the role of singlet oxygen for pollutant abatement during persulfate-based advanced oxidation processes: Co3O4@CNTs activated peroxymonosulfate as an example. *Water Res.* **244**, 120480 (2023).
11. Gligorovski, S., Strekowski, R., Barbati, S. & Vione, D. Environmental implications of hydroxyl radicals (•OH). *Chem. Rev.***115**, 13051–13092 (2015).
12. Remucal, C. K., Salhi, E., Walpen, N. & von Gunten, U. Molecular-level transformation of dissolved organic matter during oxidation by ozone and hydroxyl radical. *Environ. Sci. Technol.* **54**, 10351–10360 (2020).
13. McDonough, L. K. et al. A new conceptual framework for the transformation of groundwater dissolved organic matter. *Nat. Commun.* **13**, https://doi.org/10.1038/s41467-022-29711-9 (2022).
14. Chen, Q., Lü, F., Zhang, H., Xu, Q. Y. & He, P. J. Different Fenton treatments on diverse landfill organics: discover the underestimated effect of derived-DOM. *Water Res.* **244**, 120536 (2023).
15. Lennartz, S., Byrne, H. A., Kümmel, S., Krauss, M. & Nowak, K. M. Hydrogen isotope labeling unravels origin of soil-bound organic contaminant residues in biodegradability testing. *Nat. Commun.* **15**, 9178 (2024).
16. Vandover, C. L., Grassle, J. F., Fry, B., Garritt, R. H. & Starczak, V. R. Stable isotope evidence for entry of sewage-derived organic material into a deep-sea food web. *Nature* **360**, 153–156 (1992).
17. Medeiros, P. M. et al. Dissolved organic matter composition and photochemical transformations in the northern North Pacific Ocean. *Geophys. Res. Lett.* **42**, 863–870 (2015).
18. Mopper, K. & Zhou, X. L. Hydroxyl radical photoproduction in the sea and its potential impact on marine processes. *Science* **250**, 661–664 (1990).
19. Yuan, Z. W. et al. Molecular insights into the transformation of dissolved organic matter in landfill leachate concentrate during biodegradation and coagulation processes using ESI FT-ICR MS. *Environ. Sci. Technol.* **51**, 8110–8118 (2017).
20. Leyva, D., Tariq, M. U., Jaffé, R., Saeed, F. & Lima, F. F. Unsupervised structural classification of dissolved organic matter based on fragmentation pathways. *Environ. Sci. Technol.* **56**, 1458–1468 (2022).
21. Kim, S., Kramer, R. W. & Hatcher, P. G. Graphical method for analysis of ultrahigh-resolution broadband mass spectra of natural organic matter, the van Krevelen diagram. *Anal. Chem.* **75**, 5336–5344 (2003).
22. Rivas-Ubach, A. et al. Moving beyond the van Krevelen diagram: a new stoichiometric approach for compound classification in organisms. *Anal. Chem.* **90**, 6152–6160 (2018).
23. Zhang, B. L. et al. Transformation of dissolved organic matter during full-scale treatment of integrated chemical wastewater: molecular composition correlated with spectral indexes and acute toxicity. *Water Res.* **157**, 472–482 (2019).
24. Thavasi, V., Bettens, R. P. A. & Leong, L. P. Temperature and solvent effects on radical scavenging ability of phenols. *J. Phys. Chem. A* **113**, 3068–3077 (2009).
25. Wawer, I. & Zielinska, A. 13C-CP-MAS-NMR studies of flavonoids.: I.: solid-state conformation of quercetin, quercetin 5′-sulphonic acid

and some simple polyphenols. *Solid State Nucl. Magn. Reson.* **10**, 33–38 (1997).
26. Jia, B. et al. Antioxidant properties of larch tannins with different mean polymerization degrees: controlled degradation based on hydroxyl radical degradation. *J. Agric. Food Chem.* **70**, 9367–9376 (2022).
27. He, P. J. et al. Improvement criteria for different advanced technologies towards bio-stabilized leachate based on molecular subcategories of DOM. *J. Hazard. Mater.* **414**, 125463 (2021).
28. Zhong, Q. F. et al. Molecular level insights into HO• and Cl2•- mediated transformation of dissolved organic matter in landfill leachate concentrates during the Fenton process. *Chem. Eng. J.***446**, 137062 (2022).
29. Guo, Y., Zhan, J. H., Yu, G. & Wang, Y. J. Evaluation of the concentration and contribution of superoxide radical for micropollutant abatement during ozonation. *Water Res.* **194**, 116927 (2021).
30. Guo, Y., Yu, G., von Gunten, U. & Wang, Y. J. Evaluation of the role of superoxide radical as chain carrier for the formation of hydroxyl radical during ozonation. *Water Res.* **242**, 120158 (2023).
31. Wiegand, H. L., Orths, C. T., Kerpen, K., Lutze, H. V. & Schmidt, T. C. Investigation of the iron-peroxo complex in the Fenton reaction: kinetic indication, decay kinetics, and hydroxyl radical yields. *Environ. Sci. Technol.* **51**, 14321–14329 (2017).
32. Fischbacher, A., von Sonntag, C. & Schmidt, T. C. Hydroxyl radical yields in the Fenton process under various pH, ligand concentrations and hydrogen peroxide/Fe(II) ratios. *Chemosphere* **182**, 738–744 (2017).
33. Waggoner, D. C., Wozniak, A. S., Cory, R. M. & Hatcher, P. G. The role of reactive oxygen species in the degradation of lignin derived dissolved organic matter. *Geochim. Cosmochim. Acta* **208**, 171–184 (2017).
34. Page, S. E., Arnold, W. A. & McNeill, K. Assessing the contribution of free hydroxyl radical in organic matter-sensitized photohydroxylation reactions. *Environ. Sci. Technol.* **45**, 2818–2825 (2011).
35. Jasper, J. T. & Sedlak, D. L. Phototransformation of wastewater-derived trace organic contaminants in open-water unit process treatment wetlands. *Environ. Sci. Technol.* **47**, 10781–10790 (2013).
36. Schollée, J. E., Schymanski, E. L., Avak, S. E., Loos, M. & Hollender, J. Prioritizing unknown transformation products from biologically-treated wastewater using high-resolution mass spectrometry, multivariate statistics, and metabolic logic. *Anal. Chem.* **87**, 12121–12129 (2015).
37. He, H. et al. Photochemical transformation of dissolved organic matter in surface water augmented the formation of disinfection byproducts. *Environ. Sci. Technol.* **58**, 3399–3411 (2024).
38. Li, L. F. et al. Molecular insights into the degradation of organic matter from secondary swine wastewater effluent: a comparative study of advanced oxidation processes. *Chem. Eng. J.* **500**, 156761 (2024).
39. Schollée, J. E., Bourgin, M., von Gunten, U., McArdell, C. S. & Hollender, J. Non-target screening to trace ozonation transformation products in a wastewater treatment train including different post-treatments. *Water Res.* **142**, 267–278 (2018).
40. Buxton, G. V., Greenstock, C. L., Helman, W. P. & Ross, A. B. Critical review of rate constants for reactions of hydrated electrons, hydrogen atoms and hydroxyl radicals (•OH/•O-) in aqueous solution. *J. Phys. Chem. Ref. Data* **17**, 513–886 (1988).
41. Chan, B., O'Reilly, R. J., Easton, C. J. & Radom, L. Reactivities of amino acid derivatives toward hydrogen abstraction by •Cl and •OH. *J. Org. Chem.* **77**, 9807–9812 (2012).
42. Reissell, A., Aschmann, S. M., Atkinson, R. & Arey, J. Products of the OH radical- and O3-initiated reactions of myrcene and ocimene. *J. Geophys. Res.-Atmos.* **107**, https://doi.org/10.1029/2001jd001234 (2002).
43. Aschmann, S. M., Arey, J. & Atkinson, R. Kinetics and products of the reactions of OH radicals with cyclohexene, 1-methyl-1-cyclohexene, cis-cyclooctene, and cis-cyclodecene. *J. Phys. Chem. A* **116**, 9507–9515 (2012).
44. Varanasi, L., Coscarelli, E., Khaksari, M., Mazzoleni, L. R. & Minakata, D. Transformations of dissolved organic matter induced by UV photolysis, Hydroxyl radicals, chlorine radicals, and sulfate radicals in aqueous-phase UV-based advanced oxidation processes. *Water Res.* **135**, 22–30 (2018).
45. Schuler, R. H. & Albarran, G. The rate constants for reaction of •OH radicals with benzene and toluene. *Radiat. Phys. Chem.* **64**, 189–195 (2002).
46. Prasse, C., Ford, B., Nomura, D. K. & Sedlak, D. L. Unexpected transformation of dissolved phenols to toxic dicarbonyls by hydroxyl radicals and UV light. *Proc. Natl. Acad. Sci. USA* **115**, 2311–2316 (2018).
47. Mardyukov, A., Sanchez-Garcia, E., Crespo-Otero, R. & Sander, W. Interaction and reaction of the phenyl radical with water: a source of •OH radicals. *Angew. Chem. Int. Ed.* **48**, 4804–4807 (2009).
48. Wojnarovits, L. & Takacs, E. Structure dependence of the rate coefficients of hydroxyl radical plus aromatic molecule reaction. *Radiat. Phys. Chem.* **87**, 82–87 (2013).
49. Wojnarovits, L. & Takacs, E. Rate coefficients of hydroxyl radical reactions with pesticide molecules and related compounds: a review. *Radiat. Phys. Chem.* **96**, 120–134 (2014).
50. Wang, X. K., Wang, W. H., Wingen, L. M., Perraud, V. & Finlayson-Pitts, B. J. Top-down versus bottom-up oxidation of a neonicotinoid pesticide by •OH radicals. *Proc. Natl. Acad. Sci. USA.* **121**, https://doi.org/10.1073/pnas.2312930121 (2024).
51. Uranga, J., Mujika, J. I. & Matxain, J. M. OH oxidation toward S- and OH-containing amino acids. *J. Phys. Chem. B* **119**, 15430–15442 (2015).
52. Morelli, R., Russo-Volpe, S., Bruno, N. & Lo Scalzo, R. Fenton-dependent damage to carbohydrates: free radical scavenging activity of some simple sugars. *J. Agric. Food Chem.* **51**, 7418–7425 (2003).
53. Sugiyama, H., Hisamichi, K., Usui, T., Sakai, K. & Ishiyama, J. A study of the conformation of β-1,4-linked glucose oligomers, cellobiose to cellohexaose, in solution. *J. Mol. Struct.* **556**, 173–177 (2000).
54. Minakata, D. Development of an elementary reaction-based kinetic model to predict the aqueous-phase fate of organic compounds induced by reactive free radicals. *Acc. Chem. Res.* **57**, 1658–1669 (2024).
55. Minakata, D., Mezyk, S. P., Jones, J. W., Daws, B. R. & Crittenden, J. C. Development of linear free energy relationships for aqueous phase radical-involved chemical reactions. *Environ. Sci. Technol.* **48**, 13925–13932 (2014).
56. Minakata, D., Song, W. H., Mezyk, S. P. & Cooper, W. J. Experimental and theoretical studies on aqueous-phase reactivity of hydroxyl radicals with multiple carboxylated and hydroxylated benzene compounds. *Phys. Chem. Chem. Phys.* **17**, 11796–11812 (2015).
57. Koch, B. P. & Dittmar, T. From mass to structure: an aromaticity index for high-resolution mass data of natural organic matter. *Rapid Commun. Mass Spectrom.* **30**, 250–250 (2016).
58. An, T. C. et al. Kinetics and mechanism of •OH mediated degradation of dimethyl phthalate in aqueous solution: experimental and theoretical studies. *Environ. Sci. Technol.* **48**, 641–648 (2014).
59. Naik, G. H., Priyadarsini, K. I., Maity, A. K. & Mohan, H. One electron oxidation induced dimerization of 5-hydroxytryptophol: role of 5-hydroxy substitution. *J. Phys. Chem. A* **109**, 2062–2068 (2005).
60. Serra-Perez, E. et al. Insights into the removal of Bisphenol A by catalytic wet air oxidation upon carbon nanospheres-based catalysts: key operating parameters, degradation intermediates and reaction pathway. *Appl. Surf. Sci.* **473**, 726–737 (2019).

61. Jiang, X. et al. Insights into the role of π-electrons of aromatic aldehydes in passivating perovskite defects. *Angew. Chem. Int. Ed.* **64**, e202420369 (2024).
62. Yang, R. J., Liu, S. Y., Yin, N. Y., Zhang, Y. & Faiola, F. Tox21-based comparative analyses for the identification of potential toxic effects of environmental pollutants. *Environ. Sci. Technol.* **56**, 14668–14679 (2022).
63. Richard, A. M. et al. The Tox21 10K compound library: collaborative chemistry advancing toxicology. *Chem. Res. Toxicol.* **34**, 189–216 (2021).
64. Sipes, N. S. et al. An intuitive approach for predicting potential human health risk with the Tox21 10k library. *Environ. Sci. Technol.* **51**, 10786–10796 (2017).
65. Chen, Q., Lü, F., Zhang, H. & He, P. J. Where should Fenton go for the degradation of refractory organic contaminants in wastewater?. *Water Res.* **229**, 119479 (2023).
66. Cai, Q. Q., Lee, B. C. Y., Ong, S. L. & Hu, J. Y. Fluidized-bed Fenton technologies for recalcitrant industrial wastewater treatment-Recent advances, challenges and perspective. *Water Res.* **190**, 116692 (2021).
67. Dwinandha, D. et al. Interpretable machine learning and reactomics assisted isotopically labeled FT-ICR-MS for exploring the reactivity and transformation of natural organic matter during ultraviolet photolysis. *Environ. Sci. Technol.* **58**, 816–825 (2023).
68. Diffey, B. L. Sources and measurement of ultraviolet radiation. *Methods* **28**, 4–13 (2002).
69. Huang, W. C. et al. Influence of UV irradiation on the toxicity of chlorinated water to mammalian cells: toxicity drivers, toxicity changes and toxicity surrogates. *Water Res.* **165**, https://doi.org/10.1016/j.watres.2019.115024 (2019).
70. Qiu, J. J. et al. Persistence of native and bio-derived molecules of dissolved organic matters during simultaneous denitrification and methanogenesis for fresh waste leachate. *Water Res.* **175**, 115705 (2020).
71. Knolhoff, A. M., Kneapler, C. N. & Croley, T. R. Optimized chemical coverage and data quality for non-targeted screening applications using liquid chromatography/high-resolution mass spectrometry. *Anal. Chim. Acta* **1066**, 93–101 (2019).
72. Petras, D. et al. High-resolution liquid chromatography tandem mass spectrometry enables large scale molecular characterization of dissolved organic matter. *Front. Mar. Sci.* **4**, 405 (2017).
73. Fu, Q. L., Chen, C., Liu, Y., Fujii, M. & Fu, P. Q. FT-ICR MS spectral improvement of dissolved organic matter by the absorption mode: a comparison of the electrospray ionization in positive-ion and negative-ion modes. *Anal. Chem.* **96**, 522–530 (2023).
74. Chambers, M. C. et al. A cross-platform toolkit for mass spectrometry and proteomics. *Nat. Biotechnol.* **30**, 918–920 (2012).
75. Schum, S. K., Brown, L. E. & Mazzoleni, L. R. MFAssignR: molecular formula assignment software for ultrahigh resolution mass spectrometry analysis of environmental complex mixtures. *Environ. Res.* **191**, 110114 (2020).
76. Chen, Q., Lü, F., Qiu, J. J., Zhang, H. & He, P. J. Data for pathways and selectivity of Fenton degradation of different precursor species of dissolved organic matter. *Figshare*, https://doi.org/10.6084/m9.figshare.28190549.v1 (2025).
77. Chen, Q., Lü, F., Qiu, J. J., Zhang, H. & He, P. J. Code for pathways and selectivity of Fenton degradation of different precursor species of dissolved organic matter. *Figshare*, https://doi.org/10.6084/m9.figshare.28190588.v1 (2025).

Acknowledgements

This work was supported by the National Natural Science Foundation of China (22076145 to P.J.H.) and Shanghai Municipal Government State-Owned Assets Supervision and Administration Commission (2022028 to P.J.H.).

Author contributions

Q.C., F.L., H.Z., and P.J.H. conceived and designed the experiments; Q.C., F.L., and P.J.H. performed the experiments; Q.C., F.L., and J.J.Q. analyzed the data; Q.C., F.L., and J.J.Q. contributed materials/analysis tools and Q.C., F.L., and J.J.Q. wrote the paper.

Competing interests

The authors declare no competing interests.

Additional information

Supplementary information The online version contains supplementary material available at https://doi.org/10.1038/s41467-025-61753-7.

Correspondence and requests for materials should be addressed to Pinjing He.

Peer review information *Nature Communications* thanks Manabu Fujii, Francisco Fernandez-Lima, and the other, anonymous, reviewer(s) for their contribution to the peer review of this work. A peer review file is available.